Rapport BIPM-96/7

Measurement of air kerma and ambient dose equivalent in a ^{137}Cs beam

M. Boutillon and P. Allisy-Roberts

Bureau International des Poids et Mesures, F-92312 Sèvres CEDEX, France

Abstract. Details concerning the measurement of air kerma and ambient dose equivalent in a ^{137}Cs beam are given, together with a critical evaluation of their uncertainties.

1. Introduction

Sources of ^{137}Cs are now widely used as reference radiations, particularly in the field of radiation protection. For this reason, Section I of the Comité Consultatif pour les Etalons de Mesure des Rayonnements Ionisants (CCEMRI) recommended in 1991 that the BIPM develop a standard for air kerma and organize international comparisons of standards to ensure world-wide uniformity of measurements using caesium gamma energy. The BIPM determination of air kerma was completed in 1994, and the first international comparisons began at the same time. The BIPM also developed a standard of ambient dose equivalent at this energy for the calibration of instruments used for environmental monitoring.

A brief summary of the air kerma determination is given in [1]. In the present report, a more detailed analysis of some parameters involved is presented, together with the results of a study concerning the variation of the response of transfer chambers with geometrical conditions. In addition, the determination of the ambient dose equivalent is described.

2. Experimental arrangement

- *BIPM ^{137}Cs beam.* The ^{137}Cs source, of activity 1 TBq, is located in a lead housing. A scatter-reducing collimator [1] defines a circular beam of 11 cm diameter at 1 m from the source. This arrangement is used for measurement of air kerma. A second collimator, defining a beam of 60 cm diameter, is used for the measurement of dose equivalent at 3 m from the source. The incident beam includes a large amount of scattered radiation, the energy fluence of which, determined by calculation, amounts to about 30 % of that of the unscattered radiation. This large contribution is taken into account in the evaluation of the calculated corrections. The conditions of measurement are given in Table 1.

- *BIPM standard.* The standard of air kerma constructed at the BIPM is a cavity chamber of high-purity graphite (Table 2), of the same type as the BIPM standard used for measurements at ^{60}Co [2]. The cavity volume of the standard, 6,834 4 cm^3, has been

determined ionometrically by comparison with another standard of similar type, in both the ^{60}Co and ^{137}Cs beams. The numerical values obtained in this way differ by only 0,01 %.

Table 1. Conditions of measurement

source activity (1995)	≈ 1 TBq
source dimensions	
diameter	12 mm
length	23 mm
contribution of incident scattered radiation in terms of energy fluence	30 %
attenuation coefficients	
air (calculated)	0,0803 $cm^2 g^{-1}$
graphite (measured)	0,0806 $cm^2 g^{-1}$
measurement of air kerma	
distance from source to reference plane	1 m
beam diameter in the reference plane (first collimator)	11 cm
measurement of ambient dose equivalent	
distance from source to reference plane	3 m
beam diameter in the reference plane (second collimator)	60 cm

Table 2. Dimensions of the air kerma standard

Standard CH5-2	thickness /cm	radius /cm	ρ /(g cm^{-3})
external dimensions	1,081 5	2,50	-
half-cavity	0,206 4	2,25	-
collecting electrode	0,102 2	2,00	1,819
front wall	0,283 3	2,50	1,815
back wall	0,283 2	2,50	1,817
lateral wall	0,515 0	-	1,810
cavity volume	6,834 4 cm^3		

- *Measurements of ionization current.* Measurements of the ionization current I are carried out automatically. The value of I measured by the standard at 1 m from the source is 53 pA, with a standard deviation of 0,03 % of the mean of a series of 30 measurements. The uncertainty (of type B) in the ionization current is 0,02 %.

3. Determination of air kerma rate

The air kerma rate is given by the well-known relation

$$K = (I/m)\ (W/e)\ (1 - g)^{-1}\ (\mu_{en}/\rho)_{a,c}\ s_{c,a}\ \Pi\, k_i \quad , \qquad (1)$$

where
(I/m) is the mass ionization current measured by the standard,
W is the average energy spent by an electron of charge e to produce an ion pair in dry air ,
g is the mean fraction of electron energy lost by bremsstrahlung,
$(\mu_{en}/\rho)_{a,c}$ is the ratio of the mean mass-energy absorption coefficients of air and graphite,
$s_{c,a}$ is the ratio of the mean stopping powers of graphite and air, and
$\Pi\, k_i$ is the product of the correction factors to be applied to the standard.

3.1. Physical constants

The values of the physical constants are given in Table 3 together with their relative uncertainties, expressed as one standard deviation. The value used for W/e is that recommended by the CCEMRI [3]. The mean value of $(\mu_{en}/\rho)_{a,c}$, averaged over the photon spectrum, is calculated from the data of [4], and those of $s_{c,a}$ and g from [5]. These quantities differ by 0,2 %, 0,9 % and 0,01 %, respectively, from the values obtained for ^{137}Cs energy (0,661 2 MeV).

3.2. Correction factors

Correction factors were determined by experiment or calculation, as explained in this section. Their numerical values are summarized in Table 3, together with their uncertainties.

- *Attenuation and scattering* (k_{at} *and* k_{sc}). Attenuation and scattering effects were determined using a special chamber, of similar shape to that of the standard, but with a thin front wall of 0,85 mm, to avoid a large extrapolation to zero thickness.

The attenuation of the front wall was deduced from measurements in narrow pencil-beam conditions, by the addition of five graphite discs of various thicknesses, placed at mid-distance between the source and the chamber (Fig. 1a). The results, corrected for the scattered radiation from these discs ($8 \cdot 10^{-4}$ per cm), lead to an attenuation coefficient for graphite of 0,145 cm^{-1}, which is in good agreement with the value, 0,148 cm^{-1}, deduced from [4] for the photon beam spectrum. The discs were then placed directly in front of the chamber (Fig.1b). The contribution of the front wall to the scatter, 3,07 %, is obtained by a quadratic extrapolation of the difference between the net effect and the disc attenuation. The contribution of the back wall, 0,79 %, was determined using four additional discs placed behind the chamber (Fig. 1c). The effect of the lateral wall was first obtained by Monte-Carlo calculation and afterwards determined experimentally using three additional rings (Fig. 1d). The two values obtained, 0,49 % and 0,48 % respectively, agree well within the uncertainties.
The scattering effect of the graphite electrode, 0,46 % has been estimated from that of the chamber wall.

The total corrections for photon attenuation and scattering of the graphite are 5,4 % and 4,7 %, respectively. Although the individual values are quite large and higher than those obtained at ^{60}Co, the net effect of the photon interactions in the wall is smaller, mainly because the Compton effect is more isotropic for ^{137}Cs radiation. The uncertainty of the value of k_{sc} is mainly due to the quadratic extrapolation made for the front wall contribution and to the calculation by which the effect of the collecting electrode is estimated.

- *Mean centre of electron production* (k_{CEP}). The correction factor k_{CEP}, which takes into account the finite path of the electrons, is expressed as $k_{CEP} = 1 - \mu d_{CEP}$, where μ is the mass attenuation coefficient of graphite and d_{CEP} the depth of the mean centre of electron production [6]. The coefficient μ was measured experimentally and the value of d_{CEP}, 0,19 mm, corresponding to the multiconical sources of electrons produced in the graphite wall, was derived by the moment method [7].

- *Axial non-uniformity of the beam* (k_{an}). The correction factor for axial non-uniformity k_{an} takes into account the variation of the fluence of the primary photons over the cavity thickness and in its vicinity, due to the finite distance to the source. It has been estimated by the method used in [2] used previously for ^{60}Co. Its derivation is given in the Appendix.

- *Losses due to the recombination* (k_s). The correction factor for losses due to recombination k_s has been obtained by extrapolating to zero the reciprocal of the ionization current versus the reciprocal of the collecting voltage: only the initial recombination has been considered since volume recombination is negligible at the low kerma rate measured in the BIPM beam. The recombination effect, 0,14 %, is the same as that obtained for a low air kerma rate ^{60}Co source with another standard of the same type.

- *Radial non-uniformity of the beam* (k_{rn}). The correction factor for the non-uniformity of the beam k_{rn} amounts to 0,70 % in the reference conditions (see section 4).

- *Humidity* (k_h). The correction factor k_h which takes account of humidity, 0,997, is that recommended by the CCEMRI(I) [8].

- *Stem effect* (k_{st}). The correction factor for the influence of the stem k_{st}, which is determined experimentally using a dummy stem placed on the chamber cap opposite to the original stem, is 0,02 % at 1 m.

- *Approximation to the Bragg-Gray principle*. The cavity thickness, 2 mm, is assumed to be thin enough to fulfil the conditions of the Bragg-Gray principle. This is confirmed by the theory [9].

Table 3. Factors entering in the determination of the air kerma rate and estimated relative uncertainties

	value	100 s_i [1]	100 u_i
physical constants			
dry air density / kg m^{-3}	1,293 0 [2]	-	≤ 0,01
$(\mu_{en}/\rho)_{a,c}$	0,999 0	-	0,05
$s_{c,a}$	1,010 4	-	0,3
(W/e) / J C^{-1}	33,97	-	0,15
g	0,001 2	-	0,02
correction factors			
k_s recombination losses	1,001 4	0,01	≤ 0,01
k_h humidity	0,997 0	-	0,03
k_{st} stem scattering	0,999 8	0,01	-
k_{at} wall attenuation	1,054 0	0,01	0,04
k_{CEP} mean origin of electrons	0,997 2	-	0,01
k_{sc} wall scattering	0,953 5	0,01	0,15
k_{an} axial non-uniformity	0,998 1	-	0,07
k_{rn} radial non-uniformity	1,007 0	0,01	0,03
measurement of $I/v\rho$			
v volume / cm^3	6,834 4	0,01	0,10
I ionization current			
corrections concerning ρ (temperature, pressure, air compressibility)		0,03	0,02
relative uncertainty in K			
quadratic sum		0,04	0,40
combined uncertainty		0,40	

(1) s_i and u_i are the relative uncertainties estimated repectively by statistical methods (type A) and by other means (type B)
(2) density at 273,15 K, 101 325 Pa

The air kerma rate is 20 μGy s^{-1}. Its total uncertainty is estimated as 0,40 %. The BIPM standard of air kerma has been compared with the standards of several countries [10]. The results given in Table 4 show good agreement and are compatible with the uncertainties.

Table 4. Comparison of air kerma standards

Lab. 1-Lab. 2	$K_{Lab\ 1}/K_{Lab\ 2}$
BEV-BIPM	0,994 5
LPRI-BIPM	1,001 9
NIST-BIPM	1,001 7
OMH-BIPM	0,995 4

4. Variation of the air kerma rate with geometrical conditions

The kerma varies to some degree with the geometric conditions. Four principal causes are considered:

- *Variation with radial distance to the beam axis.* The variation of the air kerma rate in a plane perpendicular to the beam axis has been derived experimentally from measurements carried out at 1 m from the source with a small spherical chamber moved perpendicular to the beam axis. The results given in Fig. 2 show the large variation obtained when using the narrow beam. At 3 m, the beam non-uniformity is less pronounced.

- *Variation with beam diameter.* The air kerma on the beam axis, at a distance of 1 m, increases by 4,8 % when the large collimator is used in place of the narrow one. This is due to a larger fraction of scattered radiation coming from within the source housing and the collimator. At 3 m, the difference is even more pronounced, as shown in Table 5.

- *Variation with distance to the source.* The variation of the air kerma with distance to the source shows an important deviation from the inverse square law. This is due to the scattered radiation from the source housing and collimator. Table 5 shows the values of the ratio K/K_0, corrected for the inverse square law and for the distance to the source, where K_0 is the air kerma rate measured at a distance of 1 m with the narrow collimator.

Table 5. Variation of K with distance and beam diameter

	first collimator		second collimator	
distance/m	Φ beam/*cm*	K/K_0	Φ beam/*cm*	K/K_0
0,696	7,7	1,019 6		
0,971	10,7	1,000 7		
1,000	11	1,000 0	20	1,047 8
1,027	11,3	0,999 4		
3,000	33	1,006 6	60	1,068 9

- *Variation with time.* The stability of the air kerma rate corrected for decay, $T_{½}$ = 11 050 d (1 σ = 40 d) [10], is continuously checked, and a smooth decrease of about 0.1 % per year is observed, probably due to impurities influencing the half life of the caesium source (Fig. 3).

5. Calibration of instruments

- *Chamber positioning.* The standard and the chamber to be calibrated are positioned on a translation table which is moved automatically so that the chambers are placed alternately on the beam axis, in the reference plane. The air temperature is measured

with a thermistor located half way between the two chambers. To reduce the variation in temperature from external influences, the chambers and thermistor are housed in a large polystyrene box. The difference in temperature between the two chambers is less than $3 \cdot 10^{-5}$ in relative value.

- *Calibration factor*. The calibration factor N_K is given as $N_K = K/I$, where I is the ionization current measured with the transfer chamber and normalized to reference conditions. The value of K used for the calibration is taken as the mean of measurements performed with the BIPM standard before and after the calibration. Its statistical uncertainty is about $2 \cdot 10^{-4}$. The uncertainty of the calibration factor is estimated as 0,4 %.

- *Influence parameters*. The data of Table 6 show that the responses of transfer chambers do not show a significant dependence on the beam cross section. However, a substantial change, of 2,55 %, has been observed (chambers Shonka A2) between the calibration factors measured at 1m and 3 m. This could be due to additional scattering at the larger distance. The influence of the beam spectrum on the chamber response is not very significant as has been shown in [11].

Table 6. Variation of the calibration factor with geometrical conditions

distance: 1 m

chamber	$N_{K(\Phi=20\ \mathrm{cm})}/N_{K(\Phi=11\ \mathrm{cm})}$
TK 30	1,000 4
CCO1-122	1.000 2
NE 2571-2106	1,000 1
Shonka A2	1,000 5
Shonha A4-119	1,000 4
Shonka A4-231	1,000 4

6. Determination of the ambient dose equivalent

The ambient dose equivalent H^* is determined at 3 m. This is far enough from the source for the beam to be considered parallel and the photon fluence reasonably constant over a section encompassing most of the transfer chambers to be calibrated in terms of H^*. The ambient dose equivalent is given by

$$H^* = Q\,D \quad , \tag{2}$$

where Q is the quality factor and D is the absorbed dose at 1 cm below the surface of the ICRU sphere.

Since direct measurements of H^* would not be very accurate at ^{137}Cs energy, we have

chosen to obtain H^* through the measurement of air kerma and the calculation of the ratio H^*/K. This method, used in [12] for ^{60}Co, showed good consistency with experimental results. The air kerma rate is measured with the standard described above and the ratio H^*/K is obtained by the relation

$$H^*/K = Q \exp(-\mu d)\, B\, (\mu_{en}/\rho)_{ICRU,a}\, (1 - g_a)_{ICRU} \quad , \qquad (3)$$

where the exponential term is the attenuation of the primary beam over 1 cm of ICRU tissue, the term B is the ratio of the total water kerma, at a depth of 1 cm below the surface of the sphere, to that which is due to primary photons alone with B obtained by a Monte-Carlo calculation, and $(\mu_{en}/\rho)_{ICRU,a}$ is the mean ratio of mass-energy transfer coefficients in ICRU tissue and air, and g_a is the mean fraction of electron energy lost by bremsstrahlung in air .

The numerical values of these parameters are averaged over the primary beam spectrum. The calculation leads to a value H^*/K = 1,194 Sv Gy^{-1} for ^{137}Cs energy, in very good agreement with the range of values (1,18 Sv Gy^{-1} to 1,22 Sv Gy^{-1}) quoted in [12]. The value of H^*/K increases slightly, up to 1,216 Sv Gy^{-1},for the BIPM beam which includes 30 % (1 σ = 2%) of scattered radiation in terms of energy fluence. The main contribution to the uncertainty of H^*/K comes from the statistical uncertainty in the calculation of the term B and from the uncertainty of the beam-scattered component which influences all the factors in (3). The nominal value of H^* at 3 m from the source is 3,0 µSv s^{-1}, with a relative uncertainty of 0,6 % (Table 7).

Table 7. Factors entering in the determination of the ambient dose equivalent rate and estimated relative uncertainties

	numerical value	100 s_i	100 u_i
air kerma rate K		0,04	0,40
ratio H^*/K			
Q	1	-	-
$\exp(-\mu d)$	0,916 9	-	0,10
B	1,195 5	-	0,43
$(1 - g_a)_{ICRU}$	0,998 8	-	0,02
$(\mu_{en}/\rho)_{ICRU,a}$	1,110 6	-	0,10
relative uncertainty in H^*/K	1,216	-	
quadratic sum		-	0,45
combined uncertainty		0,45	
relative uncertainty in H^*			
quadratic sum		0,04	0,60
combined uncertainty		0,60	

7. Conclusion

The measurement of the air kerma rate, at 1 m from the source, is obtained at the BIPM with an uncertainty of 0,4 %, . The stability is checked periodically. The short-term reproducibility is 0,03 %, and the small long-term drift of 0,1 % per year remains constant and is most likely due to source impurities. This enables the BIPM to make international comparisons and calibrations with confidence and reliability. The first results are very promising.

Studies concerning various transfer chambers in use show that their response is quite "robust" against influence parameters, if care is taken to apply corrections when needed. Calibration in the BIPM beam is made with an uncertainty of 0,4 %.

The calibration of instruments in terms of ambient dose equivalent can be made with an uncertainty of no more than 0,6 %, due to the careful calculation of the ratio H^*/K. Since the ionization current measured by the BIPM standard at 3 m from the source is very low, the BIPM intends to make an accurate calibration of a chamber with a large volume. This will serve afterwards as a secondary standard.

Appendix

Correction factor for axial non-uniformity of the beam

Since the chamber cavity is of finite thickness and the beam not parallel, the photon fluence is not strictly the same in the front and back walls, and so neither is the fluence of the electrons which produce the ionization in the cavity. A correction factor k_{an} is thus needed. With the assumption that the fluence can be considered constant in the side wall of the chamber, k_{an} is expressed in the form [2].

$$k_{an} = 1 - 2\,(d_{CEP}/z) - u/z\,(1-f)\,F \quad ,$$

where d_{CEP}, 0,19 mm, is defined in section 3,
z is the distance to the source (1 m),
u is the thickness of each half-cavity (2 mm),
F is the fraction of the energy deposited in graphite in the forward direction, by electrons produced in the front or back wall or in the electrode; the value of F, calculated by the moment method, is 0,908, and
f is the fraction of ionization, estimated as 0,18, produced in the cavity by the electrons ejected in the lateral wall.

The resulting value of k_{an} is 0,998 1 (σ = 0,000 7). The uncertainty comes mainly from the determination of F.

References

[1] Perroche A.-M. and Boutillon M. (1995), Determination of air kerma for ^{137}Cs gamma rays, *CCEMRI(I)/93-2* (BIPM, F-92312 Sèvres CEDEX).

[2] Boutillon M. and Niatel M.T. (1973), A study of graphite cavity chamber for absolute exposure measurements of ^{60}Co gamma rays, *Metrologia* **9**, 139.

[3] BIPM (1985), Constantes physiques pour les étalons de mesure de rayonnement, *BIPM Com. Cons. Etalons Mes. Ray. Ionisants, Section (I) 8*, p R45 (Offilib, 75240 Paris Cedex 05).

[4] Hubbell J.H. (1982) Photon mass attenuation and energy-absorption coefficients from 1 keV to 20 MeV, *Intl. J. Appl. Radiat. Isot.* **33**, 1269.

[5] ICRU (1984), Stopping Powers for electrons and positrons, *ICRU Report 37* (International Commission on Radiation Units and Measurements, Bethesda, MD).

[6] Roesh W.C. (1958), Dose for nonelectronic equilibrium conditions, *Rad. Res.* **9**, 399.

[7] Boutillon M. (1968), Fonction de dissipation de l'énergie des électrons dans le carbone, *Comité International des Poids et Mesures*, Procès-Verbaux **32**, 54.

[8] BIPM (1977) , Correction d'humidité, *BIPM Com. Cons. Etalons Mes. Ray. Ionisants, Section (I) 4*, p R(6) (Offilib, 75240 Paris Cedex 05).

[9] Burlin T.E. (1968), Cavity-chamber theory, Radiation dosimetry, vol. 1, ch. 8, (Academic Press, New York)

[10] Nichols A.L. (1990), X- and gamma-ray standards for detector efficiency calibration, Nucl. Instr. Meth., A238, 467.

[11] Leitner A., Witzani J., Boutillon M., Allisy-Roberts P., Delaunay F., Lamperti P., Strachotinsky C. and Csete I., International comparisons of air kerma standards in ^{137}Cs gamma radiation, *to be published.*

[12] Perroche A.-M. and Boutillon M. (1989), Measurement of ambient dose equivalent in a ^{60}Co beam, *Rad. Prot. Dosim.*, **27**, 139.

[13] Wagner S.R., Grosswendt B., Harvey J.R., Mill A.J., Selbach H.-J and Siebert B.R.L. (1985), Unified conversion functions for the new ICRU operational radiation protection quantities, *Rad. Prot. Dosim.* **12**, 231.

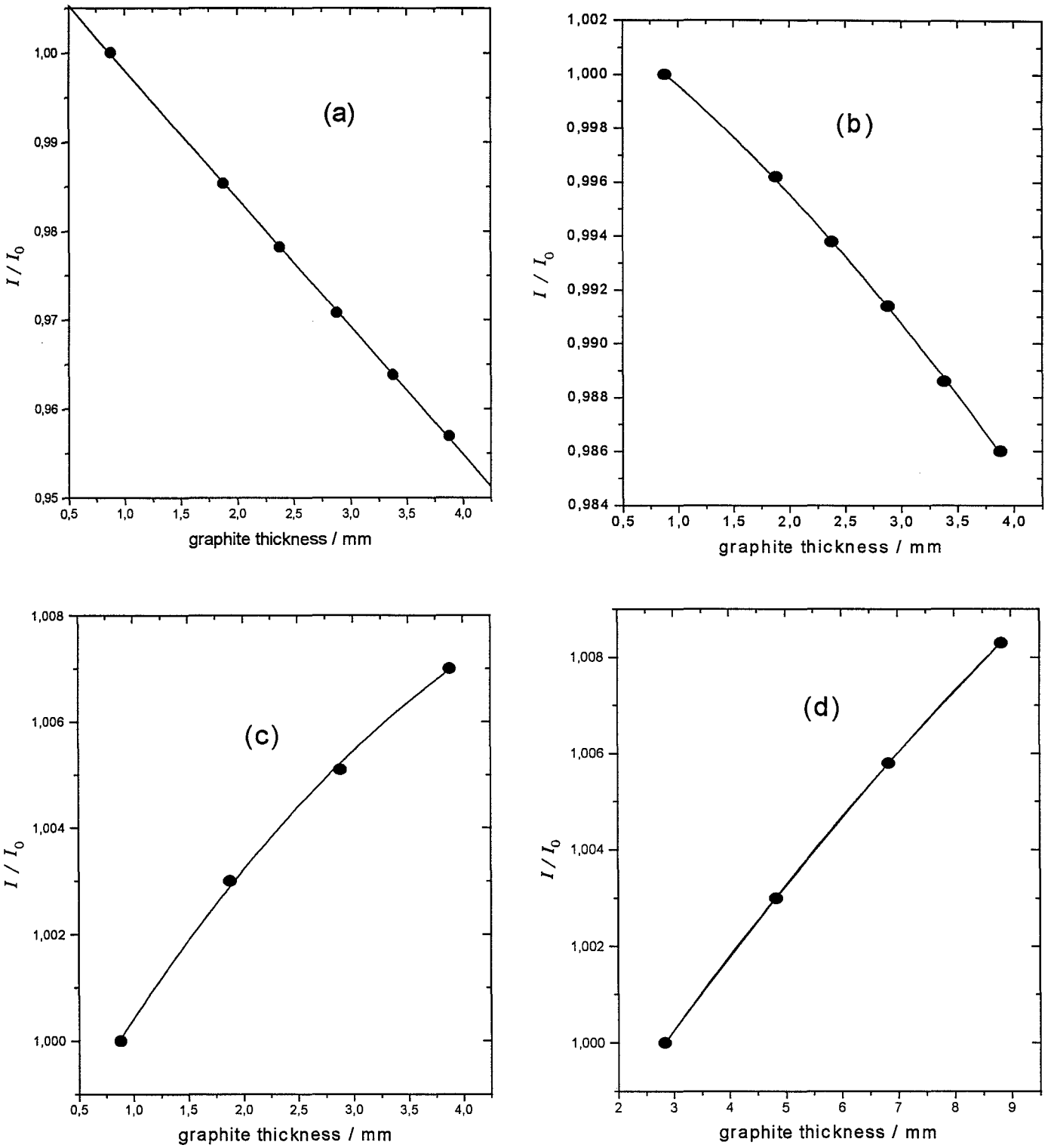

Figure 1. Variation of the ionization current I versus total graphite thickness. I_0 is the current measured without graphite disks. Graphite disks are placed on the beam axis a) far from the chamber, b) in front of the chamber, c) behind the chamber; d) rings are placed on the lateral wall.

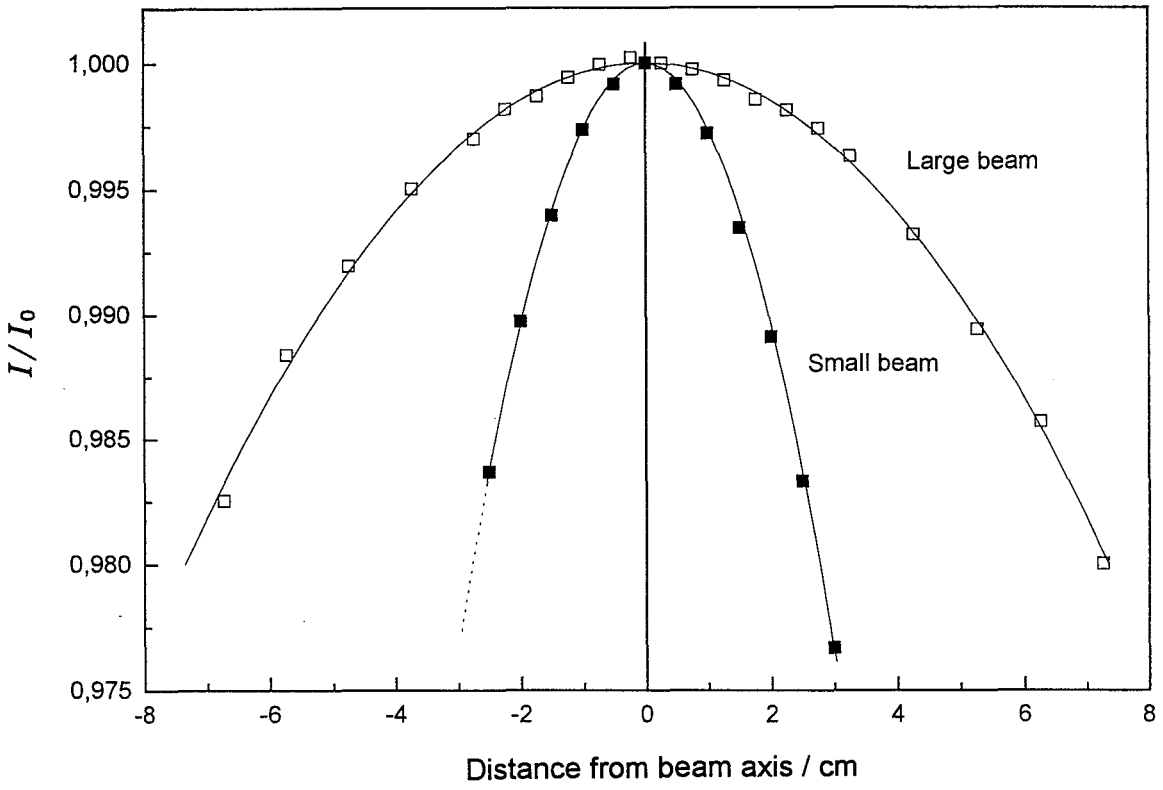

Figure 2. Variation of the ionization current I with distance to the beam axis.

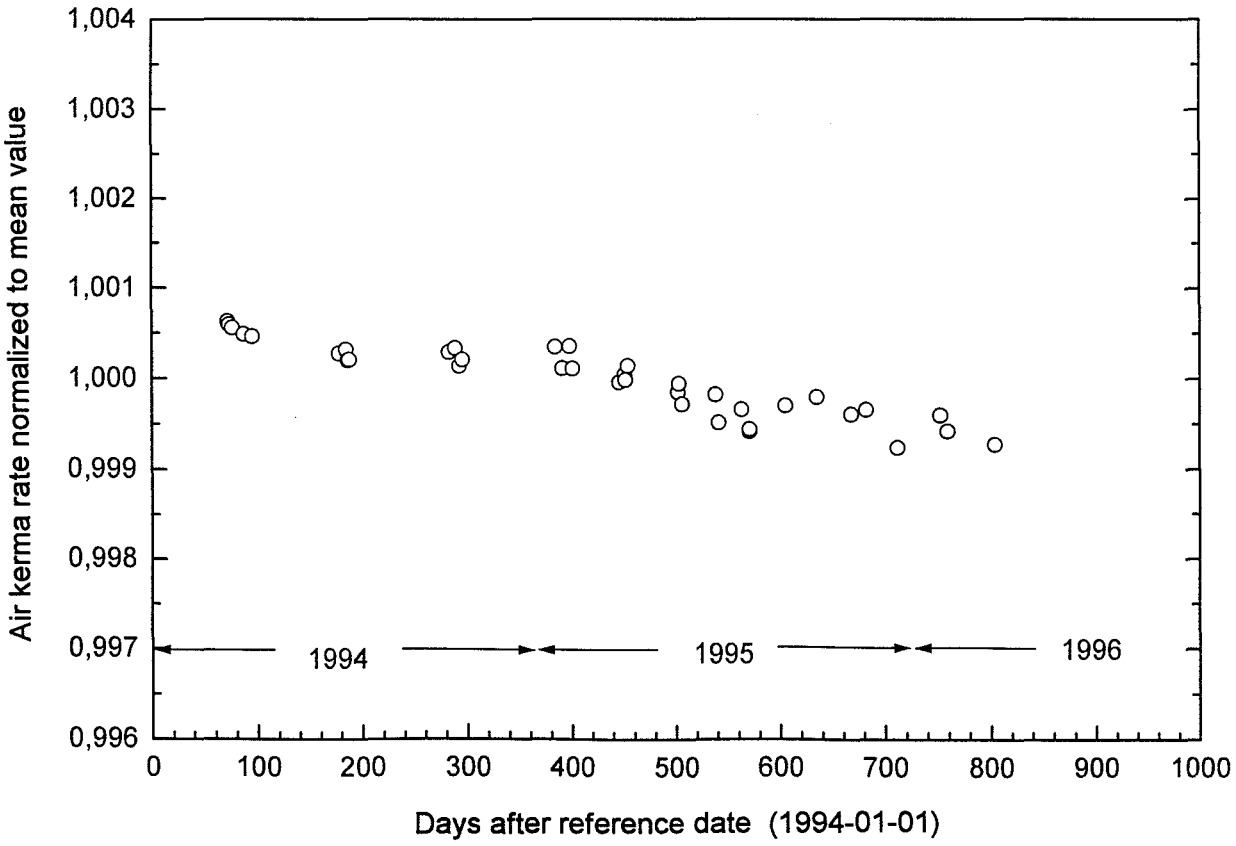

Figure 3. Variation of the air kerma rate with time